Development of Human White Matter pathways in utero over the 2nd and 3rd Trimester

Siân Wilson[a,b], Maximilian Pietsch[a], Lucilio Cordero-Grande[a,c], Anthony N Price[a], Jana Hutter[a], Jiaxin Xiao[a], Laura McCabe[a], Mary A Rutherford[a], Emer J Hughes[a], Serena J Counsell[a], Jacques-Donald Tournier[a], Tomoki Arichi[a,d,e], Joseph V Hajnal[a], A David Edwards[a,b], Daan Christiaens[a,f]*, Jonathan O'Muircheartaigh[a,g]*

[a]Centre for the Developing Brain, School of Biomedical Engineering and Imaging Sciences, King's College London, United Kingdom; [b]Centre for Neurodevelopmental Disorders, Kings College London, London, United Kingdom ; [c]Biomedical Image Technologies, ETSI Telecomunicación, Universidad Politécnica de Madrid & CIBER-BBN, Madrid, Spain; [d]Children's Neurosciences, Evelina London Children's Hospital, Guy's and St Thomas' NHS Trust, London, United Kingdom; [e]Department of Bioengineering, Imperial College London, London, United Kingdom; [f]Department of Electrical Engineering (ESAT/PSI), KU Leuven, Leuven, Belgium; [g]Department of Forensic and Neurodevelopmental Sciences & Department of Neuroimaging, Institute of Psychiatry, Psychology and Neuroscience, King's College London, London, United Kingdom

Classification: Biological sciences, Neuroscience
Key words: Fetal / Tractography / Diffusion-MRI / White matter

During the second and third trimesters of human gestation, rapid neurodevelopment is underpinned by fundamental processes including neuronal migration, cellular organisation, cortical layering and myelination. In this time, white matter growth and maturation lays the foundation for an efficient network of structural connections. Detailed knowledge about this developmental trajectory in the healthy human fetal brain is limited, in part, due to the inherent challenges of acquiring high quality MR data from this population. Here, we use state-of-the-art high-resolution multi-shell motion-corrected diffusion-weighted magnetic resonance imaging (dMRI), collected as part of the developing Human Connectome Project (dHCP) to characterize the in-utero maturation of white matter microstructure in 113 fetuses aged 22 to 37 weeks gestation. We define 5 major white matter bundles and characterize their microstructural features using both a traditional diffusion tensor and a multi-shell multi-tissue models. We found unique maturational trends in thalamocortical fibres compared to association tracts and identified different maturational trends within specific sections of the corpus callosum. Whilst linear maturational increases in FA were seen in the splenium of the corpus callosum, complex non-linear trends were seen in the majority of other white matter tracts with an initial decrease in fractional anisotropy in early gestation followed by a later increase. The latter is of particular interest as it differs markedly from the trends previously described in ex-utero preterm infants, suggesting that this normative fetal data can provide significant insights into the abnormalities in connectivity which underlie the neurodevelopmental impairments associated with preterm birth.

Significance

This work uses state-of-the-art acquisition and analysis methods developed specifically for fetal MRI to delineate the developing brain's association, projection and callosal white matter pathways. We describe unique, heterogenous maturational trajectories for different tracts, suggesting regionally distinct biological mechanisms are at play building the structural connectome *in utero*.

In the human fetus, the brain's major white matter pathways develop over the second to third trimester of gestation in an extremely rapid yet distinctly hierarchical order (1, 2). The structure and the integrity of these white matter connections have an integral role in supporting the efficiency and coordination of functional networks. Current understanding about these processes has been largely reliant on post-mortem data (2–6). Fetal MRI can capture whole-brain development in its living, functioning state, thereby providing crucial additional insight into normal growth. In the case of white matter in particular, this can include detailed investigation of developing long-range connections and region-specific trajectories.

The importance of better understanding this key period is emphasised by the high prevalence of cognitive and motor problems in children born preterm. In these infants, early exposure to the ex-utero environment likely influences later trajectories of neurodevelopment (7–9). Multiple lines of evidence suggest that white matter abnormalities are the dominant pathology, further suggesting that this specific tissue type is both at a critical stage in its development and vulnerable to external influences (10–15). In this context, characterisation of *in utero* maturation of white matter has a critical role as a normative reference.

Precise characterization of *in vivo* fetal development of white matter tracts using non-invasive methods such as MRI is challenging due to difficulties inherent to acquiring imaging data from this population, such as addressing image artifacts related to maternal tissue and constant fetal motion; as well as recruiting enough subjects to account for population heterogeneity and age effects (11, 16, 25–27, 17–24). Previous studies are also difficult to generalize as representing typical development as they have included clinical populations with brain abnormalities, or ex utero preterm infants (8, 28, 29). All existing studies have used diffusion-tensor imaging (DTI) to describe changes in microstructure (30), however the results have been inconsistent. While some studies have reported linear relationships between DTI metrics and gestational age (16, 22, 23, 31) others have fit non-linear models (18, 32) and others still have found no clear age-dependence (19, 21).

In this study, we address the limitations of DTI and challenges of fetal imaging using a state-of-the-art high angular resolution multi-shell diffusion-weighted magnetic resonance imaging (dMRI) acquisition, as well as a reconstruction and processing pipeline developed specifically for studying challenging fetal data as part of the developing Human Connectome Project (www.developingconnectome.org) (33, 34). We applied newly developed and optimised methods for *in utero* tractography and microstructure estimation in a large cohort of 113 healthy fetuses from 22 to 37 weeks gestational age (GA). With these methods we were able to delineate specific white matter bundles including the left and right corticospinal tracts (CST) (an example of a projection tract); the optic radiations (OR) and inferior longitudinal fasciculus (ILF) (examples of association tracts), and the corpus callosum (CC) (example of a commissural tract). These specific tracts were

selected due to known differences in their developmental trajectories and because their injury or abnormal development has been implicated in the pathophysiology of neurodevelopmental disorders or intellectual disability (10, 12, 35). This study represents the largest and most detailed *in-utero* characterization of maturational changes in white matter microstructure across the second to third trimester of human gestation and represents a valuable new resource for improving our understanding of the neuropathophysiology underlying neurodevelopmental disorders.

Results

Normative trends for whole brain growth and fractional anisotropy in the fetal cohort. Fetal dMRI data was collected in 151 subjects (age 22 to 38 weeks) as part of the developing Human Connectome Project (dHCP) (details presented in SI text section 1). All fetal brain images were reviewed and reported by an experienced perinatal neuroradiologist as showing appropriate appearances with no evidence of brain injury and/or malformation. Each subject was processed using the dHCP preprocessing pipeline, which includes specific measures to account for the existence of unpredictable fetal motion, geometric distortion of echo planar imaging, signal intensity inhomogeneities caused by differences in fetal position, and poor signal to noise ratio due to the small size of the fetal head and its distance from the coil (36, 37). Of the total 151 subjects that were manually assessed, 38 subjects failed due to excessive motion during acquisition (details of quality-checking criteria presented in SI text section 1).

To verify that the dataset showed normal expected trends in volumetric growth, we calculated the relationship between whole brain volume of each subject and gestational age. Consistent with existing literature, we found a strong linear increase in volume across our study period ($R2 = 0.78$, $p < 0.001$, Figure 1b) (38). Whole-brain mean FA similarly showed a positive linear relationship with gestational age (Figure 1c).

Projection, Association and Commissural White Matter Microstructure from 22-37 weeks GA. Next, we estimated individual orientation density functions (ODFs) in MRtrix3 using constrained spherical deconvolution (details presented in SI text section 2). This method improves tractography estimations by addressing the challenge of resolving crossing fiber populations within a voxel, which can confound other commonly used methods like diffusion tensor imaging (39, 40). Individual subject ODFs were first compiled into average templates for each gestational week and then probabilistic streamline tractography was used at three-weekly intervals (22, 26, 29, 32 and 35 gestational weeks) to delineate 5 different white matter pathways (splenium and genu of the corpus callosum, corticospinal tracts, inferior longitudinal fasciculi, optic radiations) (regions of interest and paths are described in SI section 3.1-3.4). Tractography was successful in all cases with the exception of the optic radiation, which was difficult to estimate in the youngest 22 gestational week template, but could be reliably identified at all other ages (Figure 2). Template-to-subject warps were then used to transform tracts from the age-matched template to individual subject space (details in section 3 SI text).

White matter bundles have distinct maturational trajectories. To place our results in the context of prior studies looking at white matter development, we first used diffusion tensor metrics; fractional anisotropy (FA) and mean diffusivity (MD) to estimate changes in the underlying microstructure of each tract. Mean FA and MD showed distinct maturational trajectories within different white matter tracts (Figure 3). The relationship between GA and tensor metrics was best described by a 2nd degree polynomial fit (as defined by Akaike Information Criterion (AIC)) in the majority of the delineated tracts (Figure 3), with the exception of FA and MD in the splenium and MD in CST where the relationship was linear (CST: FA *AIC weight (wi)* = 0.6; ILF: FA wi = 0.64, MD = 0.70; OR: FA wi = 0.72, MD = 0.73; Genu: FA wi = 0.54, MD wi = 0.71).

As expected, and in keeping with there being complex developmental changes in the white matter across our study period, relationships between FA/MD and GA were significant for all the tracts ($p < 0.01$). There were no significant differences between the left and right hemispheres for any of the delineated tracts ($p > 0.1$). Of particular interest, distinct maturational trends of FA/MD were seen within different sections of the CC; with a linear relationship between FA and GA in the splenium ($\rho = 0.36$); but a more complex relationship in the genu: with FA values first decreasing from 22 to 30 weeks GA and then increasing thereafter towards full term gestation (Figure 3). The inverse of this relationship was seen in MD values, with a linear decrease in the splenium ($\rho = -0.3$) and a similar non-linear relationship in the genu with a peak at ~30 weeks followed by a decline towards term. As with the splenium of the CC, a downward trend in FA from 22 to 30 weeks, then a steady incline from 30 weeks towards term was identified in the CST, ILF and OR (Figure 3). Similarly, inverse trends were seen in this white matter tracts in the relationship between MD and GA, with an initial rise from 22 to 30 weeks followed by a decrease towards full term. The exception was the CST which showed a strong negative correlation ($\rho = -0.75$). For completeness, the axial and radial diffusivities underlying each tract were also computed and these plots can be found in the supplementary information section.

Validating tensor metrics using multi-shell multi-tissue modelling. Given the relatively small size of the fetal brain, it is plausible that partial-voluming of tissue might have affected the estimated FA and MD values underlying the tracts, especially if streamlines traverse voxels which contain both white and grey matter or CSF (41). To specifically address these partial-voluming effects and see whether they are responsible for our observed maturational trends, we applied a multi-shell multi-tissue constrained spherical deconvolution model to the DWI data (details presented in SI text section 2), which uses the unique b-value dependencies of signal in white matter and cerebrospinal fluid to delineate intra-voxel contributions of brain tissue and fluid (11, 40). As would be expected, this analysis identified a strong positive linear trend between the fraction of fluid and mean MD in all of the delineated tracts (Figure 4) and a positive relationship between mean FA and the tissue anisotropy (Figure 4). Importantly, these linear trends suggest that the

observed non-linear maturational trends in our data cannot be attributed to simple partial voluming effects. To highlight the similarities between MD and fluid fraction trends over gestational age, a plot displaying the relationship between fluid fraction and gestational age can be found in the supplementary information (Figure S2).

Discussion

In this work, we used in utero diffusion MR imaging to report in vivo brain white matter development in a population of 113 fetuses aged 22 to 37 weeks gestation as part of the open-access developing Human Connectome Project. In addition to representing the largest ever cohort of fetuses studied in this way, we used state-of-the-art acquisition and analysis methods which have enabled the most detailed delineation of the fetal brain's white matter pathways to date. Using these methods, we have studied the brain's major association, projection and commissural fibres and demonstrate that each have distinct developmental ontogenies, with several showing non-linear changes in tract microstructure across our study period.

In accordance with post-mortem studies describing the presence of commissural and projection fibers as early as the first trimester of gestation, we were able to identify both the genu and the splenium of the corpus callosum, the CST and the ILF in our study population from 22 weeks GA onwards (Figure 2)(4, 24, 42–44). Immature axons within the cortico-cortical association tracts have also been seen as early as 15 weeks gestation, with the first appearance of the ILF reported around 15-17 weeks GA (4, 24). In our data, the only white matter tract which was challenging to delineate at the earliest 22 week GA timepoint was the optic radiation, with few streamlines reaching the back of the occipital lobe. This finding is consistent with electron microscopy studies, which report that whilst the optic radiation is evident from the lateral geniculate nucleus to the subplate by 11-13 weeks GA (45–47), synapses in the cortical plate are only evident at 23 to 25 weeks GA (46, 48).

To provide a comparison with previous studies which have reported white matter microstructural metrics derived from the widely used tensor model, we quantitively assess changes over the fetal period using FA and MD (30, 49, 50). Whilst we see linear trends in the splenium of the corpus callosum and whole brain FA, we found a more complex non-linear trend within other specific white matter bundles. In contrast to our findings, the majority of previous fetal and preterm neonatal diffusion studies have reported linear increases in FA and decreases in MD over their study periods (16, 22, 23, 31). However, many of these study populations have very few subjects under the age of 28 weeks, and some have only studied the last trimester of gestation (16, 23, 31). The reported linear increase in FA and decrease in MD in the third trimester in these previous studies therefore corresponds to the changes in FA and MD that we observe in our data between ~29 and 37 weeks in the CST, ILF, OR and splenium of the corpus callosum.

Some prior investigations into fetal white matter development have also found non-linear relationships between MD and gestational age (18, 22, 32). As with our results, Schneider et al. found that a second degree polynomial fit best described changes in MD in different white matter regions across the brain (32). Khan et al., also found an increase in MD towards 30 weeks gestation followed by a sharp decrease towards term in the cortical plate (22).

The tract-specific maturational trends we observe likely also reflect the known regional differences in white matter maturation across the brain (2, 51, 52). Tensor metrics are highly sensitive to different biological processes and therefore the unique trends we observe are likely to have resulted from a combination of multiple factors (53–55). In our data, a negative linear correlation between MD and GA was seen only in the CST and splenium which could represent simple reductions in water content and increasing fibre organization in these particular tracts over the third trimester (16, 22, 23, 31). Since histology and ex-vivo DTI studies suggest that both the CST and corpus callosum tracts are amongst the earliest to form (24, 42, 56), it is plausible based on this histological evidence that by 22 weeks gestation these tracts are already coherently organised and that MD is predominantly being affected by the reduction in water content over our study age-range. In contrast, within the ILF, OR and Genu, the initial increase in MD in could be explained by tortuous fibres becoming more coherent over this period, making water diffusion less hindered in the principle direction of the fiber pathway (18). In addition, before 30 weeks gestation there is less tissue organization and there are larger extracellular spaces between fibres to allow for cellular migration, which could further contribute to higher MD values (32). In keeping with this, histological studies have described an abundance of extracellular matrix (ECM) between white matter fiber bundles in the second trimester, which significantly decreases by 35 weeks gestation (57). Since the ECM has high water content, it is possible that its relative abundance around fibers has an effect on MD values and significantly contributes to the trends we observe.

Although FA in older cohorts is often used as a proxy for the degree of integrity or myelination, the white matter pathways in this study are still relatively immature at birth (58). Biochemical markers of mature myelin (myelin-basic protein) are largely expressed post-natally in the cerebral cortex and then increase substantially in the first two years of life (59, 60). However, unmyelinated white matter tracts still show signal intensity changes consistent with anisotropic water diffusion (61), so it is possible that the increases in FA we observe are due to active axonal outgrowth and initial ensheathment of axons by pre-myelin sheaths, generated by immature oligodendrocytes (OLs) (60, 62). In agreement with this, oligodendrocyte lineage progression has been shown to affect FA values (63) and the percentage of immature OLs in the cerebral white matter increases markedly from 30 weeks gestation (64). Back et al., also identify the first signs of pre-oligodendrocyte ensheathment of axons at approximately 30 weeks gestation (62), coinciding with the transition in our FA trends for the CST, ILF, OR and Genu. Of further interest, Xu et al., 2014 also identified 30-31 weeks gestation as a transitional point from HARDI-defined radial coherence to cortico-cortical coherence, indicating the emergence of cortico-cortical association fibres (65). These MRI findings were correlated with

histology, where they additionally observed the transformation of radial glial fibres into astrocytes (65). Together, these observations indicate that there are several developmental processes that transition around 30 weeks gestation which are likely to have had an effect on the FA values and are contributing to the unique trends we describe in Figure 3.

Our results additionally support existing evidence that there is heterogeneity in the development of the different compartments of the corpus callosum (59). In our data, the precise neurobiological underpinnings of these differing trajectories between the genu and the splenium cannot be determined just with diffusion MRI data alone. Developing callosal fibers grow through complex pathways and cross the midline using different substrates in transient fetal structures such as the callosal septa. The callosal septa are prominent between 18-34 weeks and their biochemical composition is dynamically over this period, including changes in the expression of axonal guidance molecules, cellular and extracellular matrix constituents, which are likely to affect tensor metrics (66, 67). Previous studies have also identified differences in the growth rate of different sections of the CC; with the genu growing at a faster rate than the body and the splenium during fetal development; but then after birth, mature myelination is observed in the splenium before the genu (56, 59, 68, 69). Kinney et al additionally report a difference in the delay between the onset and maturation of myelin between the anterior and posterior sections of the corpus callosum, which might further contribute to the different trends we observe in FA/MD between the two distinct sections. Therefore, it is possible that the initial higher FA values in the genu at 22 weeks are reflective of a faster growth rate over the fetal period. The pre-myelin phase then initiates first in the splenium, resulting in a higher FA in comparison to the genu at full term age (59). Based on our findings, future studies would benefit from further delineation of the corpus callosum into different compartments through combination with histology, for more specificity.

Developing white matter is known to be vulnerable to adverse influences related to the extrauterine environment and early damage lead to significant life-long neurocognitive impairments (7, 70, 71). A comprehensive characterization of in utero normal white matter development is therefore a critically important reference point for comparison with data from preterm infants. In addition to enabling more detailed and reliable tractography, continuing advances in dMRI imaging and processing pipelines can also now provide more information about the underlying microstructural changes. This can give new insight into the mechanisms of white matter injury, such as why certain tracts appear more susceptible to damage than others and how this is influenced by timing of the related insult (55, 72, 73). In a wider sense, the combination of in utero dMRI with ex utero imaging and histological studies can therefore provide a comprehensive understanding about the role of aberrant early development in the pathophysiology of neurodevelopmental disorders originating in the perinatal period.

To address partial-voluming effects and understand if they could explain the trends seen in our data, we applied a multi-shell multi-tissue constrained spherical deconvolution model, which uses the unique b-value dependencies of signal in white matter and cerebrospinal fluid to delineate intra-voxel contributions of brain tissue and fluid (40, 74). In adults, this more complex approach to modelling voxel-wise diffusion has been shown to improve the precision of fiber orientation estimations at tissue interfaces (75). As seen in neonatal cohorts, partial voluming between tissue and fluid is present in fetal dMRI data to varying degrees throughout the brain and as a function of maturation (34). In the tissue specific ODFs, we found a strong positive linear relationship in all tracts between the mean MD value and the fluid fraction, verifying the expected relationship between MD and voxel-wise fluid density. Based on this result, we propose that partial voluming effects alone cannot explain the observed non-linear “U” shaped relationships between gestational age and FA and MD values.

The image acquisition and processing pipelines used in this study were specifically designed to address the unique challenges associated with fetal and neonatal neuroimaging within the Developing Human Connectome Project (http://www.developingconnectome.org/). The advances within this project have both significantly reduced data loss and markedly increased the signal to noise ratio and sensitivity, ultimately offering improved biological interpretation. Whilst there is a large body of literature to support that measuring white matter structural integrity with diffusion tensor imaging has clinical relevance (53, 55, 73, 76), tensor metrics do not provide direct visualization of fiber bundles and therefore findings must be complemented by existing knowledge from histology. However, the non-invasive nature of dMRI allows whole-brain 3D visualization, thus enabling studies investigating the development of long-range connectivity across the entire brain network and comparisons of regional differences in brain development. Through combining state-of-the-art acquisition and methodology, we have sufficient sensitivity to highlight different developmental trajectories within specific white matter tracts and in doing so provide valuable new insights about a fundamental stage in early human brain development.

In summary, we describe the largest study to date in a healthy fetal cohort using diffusion MRI methods to characterise the fundamental processes underlying healthy white matter development across the late second to third trimesters of human gestation. Our large cohort covers a wide age range and only includes healthy fetuses with no evidence of brain injury, which is in marked contrast to previous reports that have studied narrower windows in development and included fetuses with abnormalities. Our results and the associated data represent a valuable resource representative of healthy white matter development in utero which can be compared to that of clinical populations at risk of neurodevelopmental difficulties such as those born preterm.

Methods. Fetal dMRI data was collected in 151 subjects as part of the Developing Human Connectome Project (dHCP) (Figure 1a). Raw data were pre-processed using a bespoke pipeline (details described in SI text) that includes denoising, bias

correction, dynamic distortion correction and slice-to-volume motion. Only images that passed quality control were included in this study.

For each subject, the *b=0* and *b=1000* volumes were extracted and used to estimate the diffusion tensor and calculate FA/MD maps (details in SI text).
We then estimated ODFs for each subject in MRtrix3 (www.mrtrix3.org) Individual subject ODFs were compiled into weekly templates (details in SI text). Probabilistic streamline tractography was used to estimate the 5 different tracts, streamlines were guided by specific seed regions, waypoints and exclusion zones based on the known neuroanatomy of the tracts (details in SI text). Tracts were overlaid onto the FA and MD maps and then the mean FA and MD values were calculated within the overlaid streamlines. The Akaike information criterion (AIC) (77) was used to evaluate the most suitable model across different degrees of polynomial fit (1-4), to describe the relationship between gestational age and FA/MD.

To model the data using a multi-shell multi-tissue approach, subject-specific WM response functions were extracted and the oldest 20 subjects were averaged to obtain a group-average response function of relatively mature WM (details in SI text). A group-average CSF response function was calculated from the whole cohort of subjects. All subjects' dMRI signal was deconvolved into tissue ODF and fluid components using multi-shell multi-tissue constrained spherical deconvolution and the two corresponding group-average response functions. Tracts were overlaid onto the normalised fluid ODF (to approximate the fluid fraction in each voxel), and onto the square root of the power in the l=2 band of the tissue ODF (representing tissue anisotropy). The mean CSF fraction and mean tissue anisotropy for each tract was calculated.

Acknowledgements. The authors thank the patients who agreed to participate in this work and the staff of St Thomas' Hospital London. This work was supported by the European Research Council under the European Union Seventh Framework Programme (FP/2007-2013)/ERC Grant Agreement no. 319456. The authors acknowledge infrastructure support from the National Institute for Health Research (NIHR) Mental Health Biomedical Research Centre (BRC) at South London, Maudsley NHS Foundation Trust, King's College London and the NIHR-BRC at Guys and St Thomas' Hospitals NHS Foundation Trust (GSTFT). The authors also acknowledge support in part from the Wellcome Engineering and Physical Sciences Research Council (EPSRC) Centre for Medical Engineering at King's College London [WT 203148/Z/16/Z] and the Medical Research Council (UK) [MR/K006355/1 and MR/L011530/1]. J.O.M. is supported by a Sir Henry Dale Fellowship jointly funded by the Wellcome Trust and the Royal Society (Grant Number 206675/Z/17/Z). J.O.M. and A.D.E. received support from the Medical Research Council Centre for Neurodevelopmental Disorders, King's College London (grant MR/N026063/1). TA was supported by a MRC Clinician Scientist Fellowship [MR/P008712/1]. Support for this work was also provided by the National Institute for Health Research (NIHR) Biomedical Research Centre (BRC) at Kings College London, Guy's and St Thomas' National Health Service Foundation Trust in partnership with King's College London and King's College Hospital NHS Foundation Trust.

Authors declare no competing interest
Corresponding author: Dr. Tomoki Arichi. E-mail: tom.arichi@kcl.ac.uk

References

1. E. . Gilles, Floyd H. Leviton, A. Dooling, The Developing Human Brain: Growth and Epidemiologic Neuropathology - F. H. Gilles, A. Leviton, E. C. Dooling - Google Books (1983) (June 24, 2020).
2. B. A. Brody, H. C. Kinney, A. S. Kloman, F. H. Gilles, Sequence of central nervous system myelination in human infancy. I. An autopsy study of myelination. *J. Neuropathol. Exp. Neurol.* **46**, 283–301 (1987).
3. L. A. Yakovlev PL, Yakovlev PL, Lecours AR (1967) The myelogenetic cycles of regional maturation of the brain. In: Resional development of the brain in early life (Minkowski A, eds), pp 3-70. Oxford: Blackwell. (1967) (June 24, 2020).
4. I. Kostović, M. Judaš, Prolonged coexistence of transient and permanent circuitry elements in the developing cerebral cortex of fetuses and preterm infants. *Dev. Med. Child Neurol.* **48**, 388–393 (2006).
5. I. Kostović, N. Jovanov-Milošević, The development of cerebral connections during the first 20-45 weeks' gestation. *Semin. Fetal Neonatal Med.* **11**, 415–422 (2006).
6. S. A. Bayer, J. Altman, *The Human Brain During the Second Trimester - Shirley A. Bayer, Joseph Altman - Google Books* (2005) (June 24, 2020).
7. A.-M. Childs, *et al.*, American Journal of Neuroradiology. *Am. J. Neuroradiol.* **20**, 1349–1357 (2001).
8. L. C. Maas, *et al.*, Early laminar organization of the human cerebrum demonstrated with diffusion tensor imaging in extremely premature infants. *Neuroimage* **22**, 1134–1140 (2004).
9. S. A. Back, White matter injury in the preterm infant: pathology and mechanisms. *Acta Neuropathol.* **134**, 331–349 (2017).
10. J. J. Volpe, Brain injury in premature infants: a complex amalgam of destructive and developmental disturbances. *Lancet Neurol.* **8**, 110–124 (2009).
11. D. Batalle, *et al.*, Early development of structural networks and the impact of prematurity on brain connectivity. *Neuroimage* **149**, 379–392 (2017).
12. C. Nosarti, *et al.*, Preterm birth and structural brain alterations in early adulthood. *NeuroImage Clin.* **6**, 180–191 (2014).
13. M. Allin, *et al.*, Cognitive maturation in preterm and term born adolescents. *J. Neurol. Neurosurg. Psychiatry* **79**, 381–386 (2008).
14. L. J. Woodward, J. O. Edgin, D. Thompson, T. E. Inder, Object working memory deficits predicted by early brain injury and development in the preterm infant. *Brain* **128**, 2578–2587 (2005).
15. B. Larroque, *et al.*, Neurodevelopmental disabilities and special care of 5-year-old children born before 33 weeks of gestation (the EPIPAGE study): a longitudinal cohort study. *Lancet* **371**, 813–820 (2008).
16. T. Bui, *et al.*, Microstructural development of human brain assessed in utero by diffusion tensor imaging. *Pediatr. Radiol.* **36**, 1133–1140 (2006).
17. G. Kasprian, *et al.*, In utero tractography of fetal white matter development. *Neuroimage* **43**, 213–224 (2008).
18. E. Zanin, *et al.*, White matter maturation of normal human fetal brain. An in vivo diffusion tensor tractography study. *Brain Behav.* **1**, 95–108 (2011).
19. C. Mitter, D. Prayer, P. C. Brugger, M. Weber, G. Kasprian, In Vivo Tractography of Fetal Association Fibers (2015) https:/doi.org/10.1371/journal.pone.0119536.
20. A. Jakab, R. Tuura, C. Kellenberger, I. Scheer, In utero diffusion tensor imaging of the fetal brain: A reproducibility study. *NeuroImage Clin.* **15**, 601–612 (2017).
21. G. Lockwood Estrin, *et al.*, White and grey matter development in utero assessed using motion-corrected diffusion tensor imaging and its comparison to ex utero measures. *Magn. Reson. Mater. Physics, Biol. Med.* **32**, 473–485 (2019).
22. S. Khan, *et al.*, Fetal brain growth portrayed by a spatiotemporal diffusion tensor MRI atlas computed from in utero images. *Neuroimage* **185**, 593–608 (2019).
23. C. Jaimes, *et al.*, In vivo characterization of emerging white matter microstructure in the fetal brain in the third trimester. *Hum. Brain Mapp.* **41**, 3177–3185 (2020).
24. H. Huang, *et al.*, White and gray matter development in human fetal, newborn and pediatric brains. *Neuroimage* **33**, 27–38 (2006).
25. H. Huang, L. Vasung, Gaining insight of fetal brain development with diffusion MRI and histology. *Int. J. Dev. Neurosci.* (2014) https:/doi.org/10.1016/j.ijdevneu.2013.06.005.
26. D. Batalle, *et al.*, Different patterns of cortical maturation before and after 38 weeks gestational age demonstrated by diffusion MRI in vivo (2019) https:/doi.org/10.1016/j.neuroimage.2018.05.046 (November 28, 2019).
27. J. H. Gilmore, R. C. Knickmeyer, W. Gao, Imaging structural and functional brain development in early childhood. *Nat. Rev. Neurosci.* **19**, 123–137 (2018).
28. R. C. McKinstry, *et al.*, Radial organization of developing preterm human cerebral cortex revealed by non-invasive water diffusion anisotropy MRI. *Cereb. Cortex* **12**, 1237–1243 (2002).
29. P. S. Hüppi, *et al.*, Microstructural development of human newborn cerebral white matter assessed in vivo by diffusion tensor magnetic resonance imaging. *Pediatr. Res.* **44**, 584–590 (1998).
30. P. J. Basser, J. Mattiello, D. LeBihan, MR diffusion tensor spectroscopy and imaging. *Biophys. J.* **66**, 259–267 (1994).
31. K. Keunen, *et al.*, Early human brain development: insights into macroscale connectome wiring. *Pediatr. Res.* **84**, 829–836 (2018).
32. J. F. Schneider, *et al.*, Diffusion-weighted imaging in normal fetal brain maturation. *Eur. Radiol.* **17**, 2422–2429 (2007).
33. E. J. Hughes, *et al.*, A dedicated neonatal brain imaging system. *Magn. Reson. Med.* **78**, 794–804 (2017).
34. M. Pietsch, *et al.*, A framework for multi-component analysis of diffusion MRI data over the neonatal period. *Neuroimage* **186**, 321–337 (2019).
35. J. O'Muircheartaigh, *et al.*, Modelling brain development to detect white matter injury in term and preterm born neonates. *Brain* **143**, 467–479 (2020).

36. D. Christiaens, *et al.*, Scattered slice SHARD reconstruction for motion correction in multi-shell diffusion MRI. *Neuroimage* **225**, 117437 (2021).
37. M. Deprez, *et al.*, Higher Order Spherical Harmonics Reconstruction of Fetal Diffusion MRI with Intensity Correction. *IEEE Trans. Med. Imaging* **39**, 1104–1113 (2020).
38. A. Gholipour, *et al.*, Fetal brain volumetry through MRI volumetric reconstruction and segmentation. *Int J CARS* **6**, 329–339 (2011).
39. J. D. Tournier, F. Calamante, A. Connelly, Robust determination of the fibre orientation distribution in diffusion MRI: Non-negativity constrained super-resolved spherical deconvolution. *Neuroimage* **35**, 1459–1472 (2007).
40. B. Jeurissen, J. D. Tournier, T. Dhollander, A. Connelly, J. Sijbers, Multi-tissue constrained spherical deconvolution for improved analysis of multi-shell diffusion MRI data. *Neuroimage* **103**, 411–426 (2014).
41. A. L. Alexander, K. M. Hasan, M. Lazar, J. S. Tsuruda, D. L. Parker, Analysis of partial volume effects in diffusion-tensor MRI. *Magn. Reson. Med.* **45**, 770–780 (2001).
42. H. Huang, *et al.*, Anatomical Characterization of Human Fetal Brain Development with Diffusion Tensor Magnetic Resonance Imaging (2009) https:/doi.org/10.1523/JNEUROSCI.2769-08.2009 (November 6, 2019).
43. E. Takahashi, R. D. Folkerth, A. M. Galaburda, P. E. Grant, Emerging cerebral connectivity in the human fetal Brain: An MR tractography study. *Cereb. Cortex* **22**, 455–464 (2012).
44. J. Dubois, *et al.*, The early development of brain white matter: A review of imaging studies in fetuses, newborns and infants. *Neuroscience* **276**, 48–71 (2014).
45. P. Rakic, Prenatal development of the visual system in rhesus monkey. *Philos. Trans. R. Soc. London. Ser. B Biol. Sci.* **278**, 245–260 (1977).
46. I. Kostovic, P. Rakic, Developmental history of the transient subplate zone in the visual and somatosensory cortex of the macaque monkey and human brain. *J. Comp. Neurol.* **297**, 441–470 (1990).
47. J. A. De Carlos, D. D. M. O'Leary, Growth and targeting of subplate axons and establishment of major cortical pathways. *J. Neurosci.* **12**, 1194–1211 (1992).
48. M. E. Molliver, I. Kostović, H. Van Der Loos, The development of synapses in cerebral cortex of the human fetus. *Brain Res.* **50**, 403–407 (1973).
49. P. J. Basser, J. Mattiello, D. Lebihan, Estimation of the Effective Self-Diffusion Tensor from the NMR Spin Echo. *J. Magn. Reson. Ser. B* **103**, 247–254 (1994).
50. S. K. Song, *et al.*, Dysmyelination revealed through MRI as increased radial (but unchanged axial) diffusion of water. *Neuroimage* **17**, 1429–1436 (2002).
51. H. C. Kinney, B. A. Brody, A. S. Kloman, F. H. Gilles, Sequence of central nervous system myelination in human infancy: II. Patterns of myelination in autopsied infants. *J. Neuropathol. Exp. Neurol.* **47**, 217–234 (1988).
52. J. S. Bolton, Anatomie des menschlichen Gehirns und Ruckenmarks auf myelogenetsher Gründlage. By Paul Flechsig. Erster Band. Leipsig: Georg Thieme, 1920. Demy 4to. Pp. 121, with 25 plates and 8 figures. Price £1 6 s . 8 d . . *J. Ment. Sci.* (1921) https:/doi.org/10.1192/bjp.67.277.210.
53. P. S. Hüppi, *et al.*, Microstructural development of human newborn cerebral white matter assessed in vivo by diffusion tensor magnetic resonance imaging. *Pediatr. Res.* **44**, 584–590 (1998).
54. P. Mukherjee, *et al.*, Normal brain maturation during childhood: Developmental trends characterized with diffusion-tensor MR imaging. *Radiology* **221**, 349–358 (2001).
55. J. Neil, J. Miller, P. Mukherjee, P. S. Hüppi, Diffusion tensor imaging of normal and injured developing human brain - A technical review. *NMR Biomed.* **15**, 543–552 (2002).
56. P. Rakic, P. I. Yakovlev, Development of the corpus callosum and cavum septi in man. *J. Comp. Neurol.* **132**, 45–72 (1968).
57. R. I. Milos, *et al.*, Developmental dynamics of the periventricular parietal crossroads of growing cortical pathways in the fetal brain – In vivo fetal MRI with histological correlation. *Neuroimage* **210**, 116553 (2020).
58. J. J. Volpe, *et al.*, *Volpe's neurology of the newborn* (2017) https:/doi.org/10.1016/c2010-0-68825-0.
59. H. C. Kinney, B. A. Brody, A. S. Kloman, F. H. Gilles, Sequence of central nervous system myelination in human infancy: II. Patterns of myelination in autopsied infants. *J. Neuropathol. Exp. Neurol.* **47**, 217–234 (1988).
60. R. L. Haynes, *et al.*, Axonal development in the cerebral white matter of the human fetus and infant. *J. Comp. Neurol.* **484**, 156–167 (2005).
61. D. M. Wimberger, *et al.*, Identification of "premyelination" bydiffusion-weighted mri. *J. Comput. Assist. Tomogr.* **19**, 28–33 (1995).
62. S. A. Back, N. L. Luo, N. S. Borenstein, J. J. Volpe, H. C. Kinney, Arrested oligodendrocyte lineage progression during human cerebral white matter development: Dissociation between the timing of progenitor differentiation and myelinogenesis. *J. Neuropathol. Exp. Neurol.* **61**, 197–211 (2002).
63. A. Drobyshevsky, *et al.*, Developmental changes in diffusion anisotropy coincide with immature oligodendrocyte progression and maturation of compound action potential. *J. Neurosci.* **25**, 5988–5997 (2005).
64. S. A. Back, *et al.*, Late oligodendrocyte progenitors coincide with the developmental window of vulnerability for human perinatal white matter injury. *J. Neurosci.* **21**, 1302–1312 (2001).
65. G. Xu, *et al.*, Radial coherence of diffusion tractography in the cerebral white matter of the human fetus: Neuroanatomic insights. *Cereb. Cortex* **24**, 579–592 (2014).
66. M. Culjat, N. J. Milošević, Callosal septa express guidance cues and are paramedian guideposts for human corpus callosum development. *J. Anat.* **235**, 670–686 (2019).
67. N. Jovanov-Milošević, V. Benjak, I. Kostović, Transient cellular structures in developing corpus callosum of the human brain. *Coll. Antropol.* (2006).
68. R. Achiron, A. Achiron, Development of the human fetal corpus callosum: A high-resolution, cross-sectional sonographic study. *Ultrasound Obstet. Gynecol.* (2001) https:/doi.org/10.1046/j.0960-7692.2001.00512.x.
69. A. J. Barkovich, B. O. Kjos, D. E. Jackson, D. Norman, Normal maturation of the neonatal and infant brain: MR imaging at 1.5 T. *Radiology* **166**, 173–180 (1988).
70. O. Kapellou, *et al.*, Abnormal cortical development after premature birth shown by altered allometric scaling of brain growth. *PLoS Med.* (2006) https:/doi.org/10.1371/journal.pmed.0030265.
71. C. Raybaud, T. Ahmad, N. Rastegar, M. Shroff, M. Al Nassar, The premature brain: Developmental and lesional anatomy. *Neuroradiology* **55** (2013).
72. J. J. Volpe, A. Zipurksy, Neurobiology of periventricular leukomalacia in the premature infant. *Pediatr. Res.* (2001) https:/doi.org/10.1203/00006450-200111000-00003.
73. P. S. Hüppi, *et al.*, Microstructural brain development after perinatal cerebral white matter injury assessed by diffusion tensor magnetic resonance imaging. *Pediatrics* **107**, 455–460 (2001).
74. J. D. Tournier, *et al.*, MRtrix3: A fast, flexible and open software framework for medical image processing and visualisation. *Neuroimage* **202** (2019).
75. K. G. Schilling, *et al.*, Histological validation of diffusion MRI fiber orientation distributions and dispersion. *Neuroimage* **165**, 200–221 (2018).
76. S. P. Miller, *et al.*, Serial quantitative diffusion tensor MRI of the premature brain: Development in newborns with and without injury. *J. Magn. Reson. Imaging* **16**, 621–632 (2002).
77. H. Akaike, Information theory and an extension of the maximum likelihood principle. Proceedings of the 2nd international symposium on information theory. *Second Int. Symp. Inf. Theory* (1973).

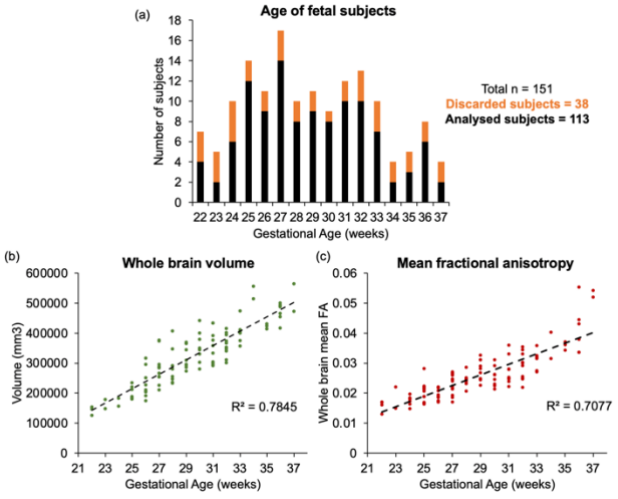

Figure 1 (a) Distribution of subjects used in the study according to their gestational age (black), including those discarded at the tractography stage (orange). (b) The whole brain volume of each subject plotted according to GA. (c) The mean FA across the whole brain in each subject, plotted according to GA.

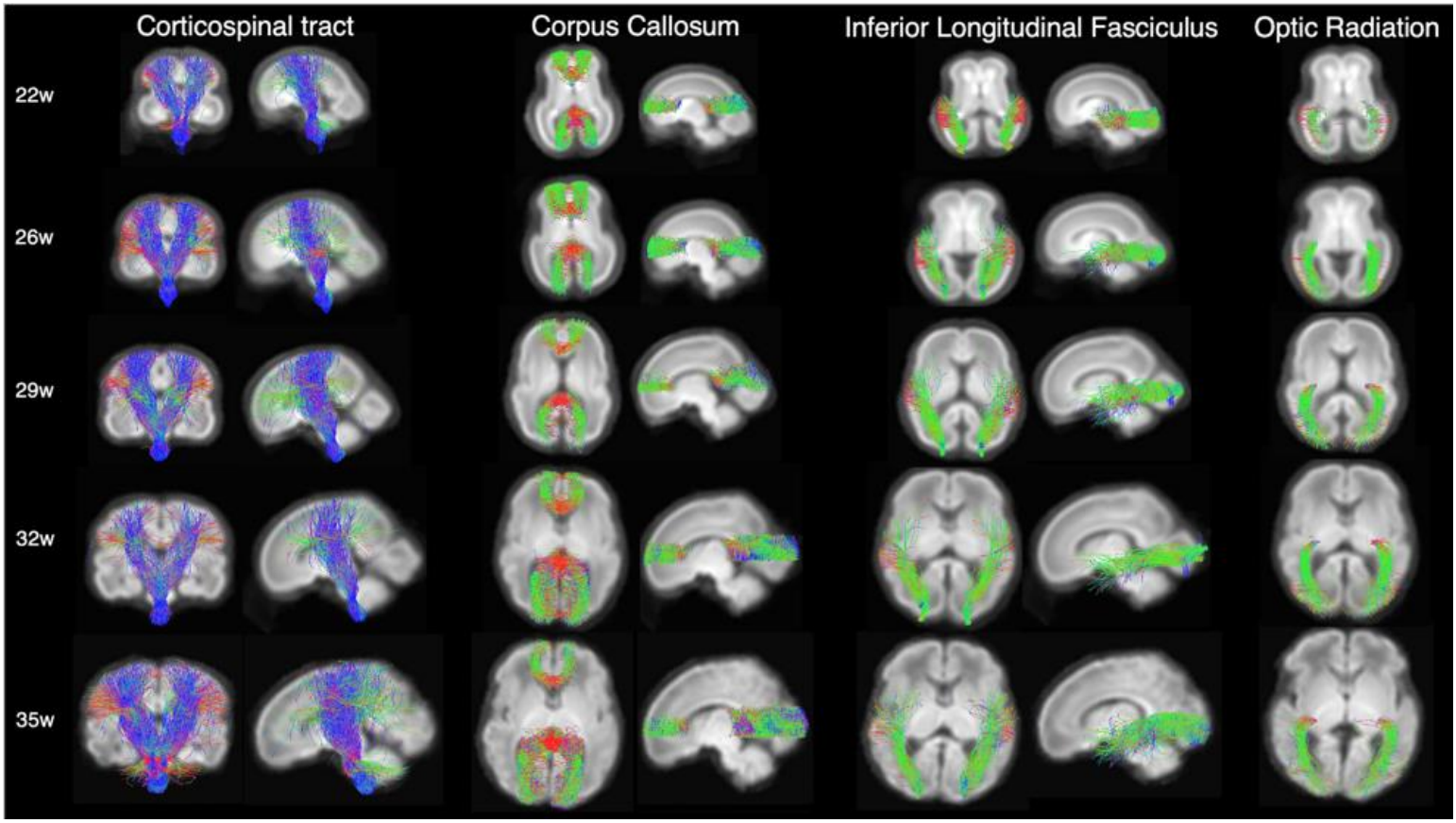

Figure 2. White matter pathways estimated using targeted probabilistic streamline tractography in orientation density function (ODF) templates constructed by averaging individual subject ODFs for each gestational week. The color-coding of tractography connections is based on a standard red-green-blue (RGB) code applied to the vector between the end-points of each structure (green for anterior–posterior, red for right–left and blue for dorsal–ventral)

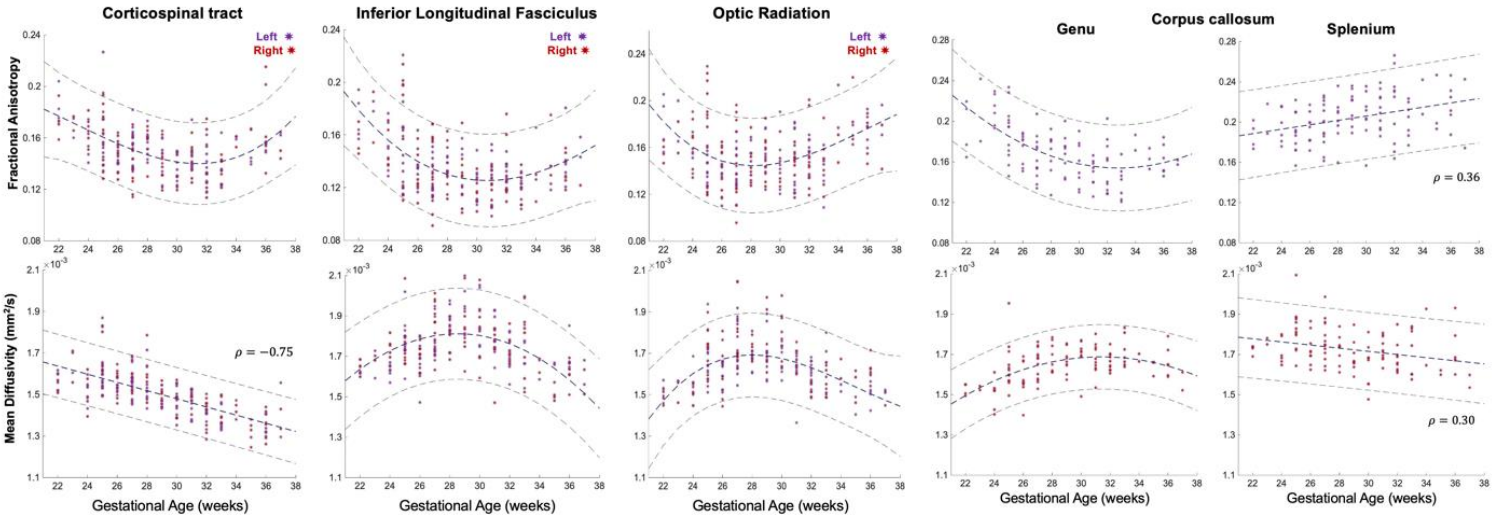

Figure 3. Mean FA and MD values underlying the left (red) and right (purple) CST, ILF, OR, Genu and Splenium for each fetal subject, plotted according to the gestational age of the subject in weeks. A second degree polynomial curve is fitted for the FA in the CST, ILF, OR and Genu, the MD in the ILF, OR and Genu (navy dashed line). The MD in the CST and the FA/MD in the splenium have linear relationships with gestational age, described by a Spearman's rank correlation coefficient (ρ). Dashed lines above and below represent the 95% confidence interval.

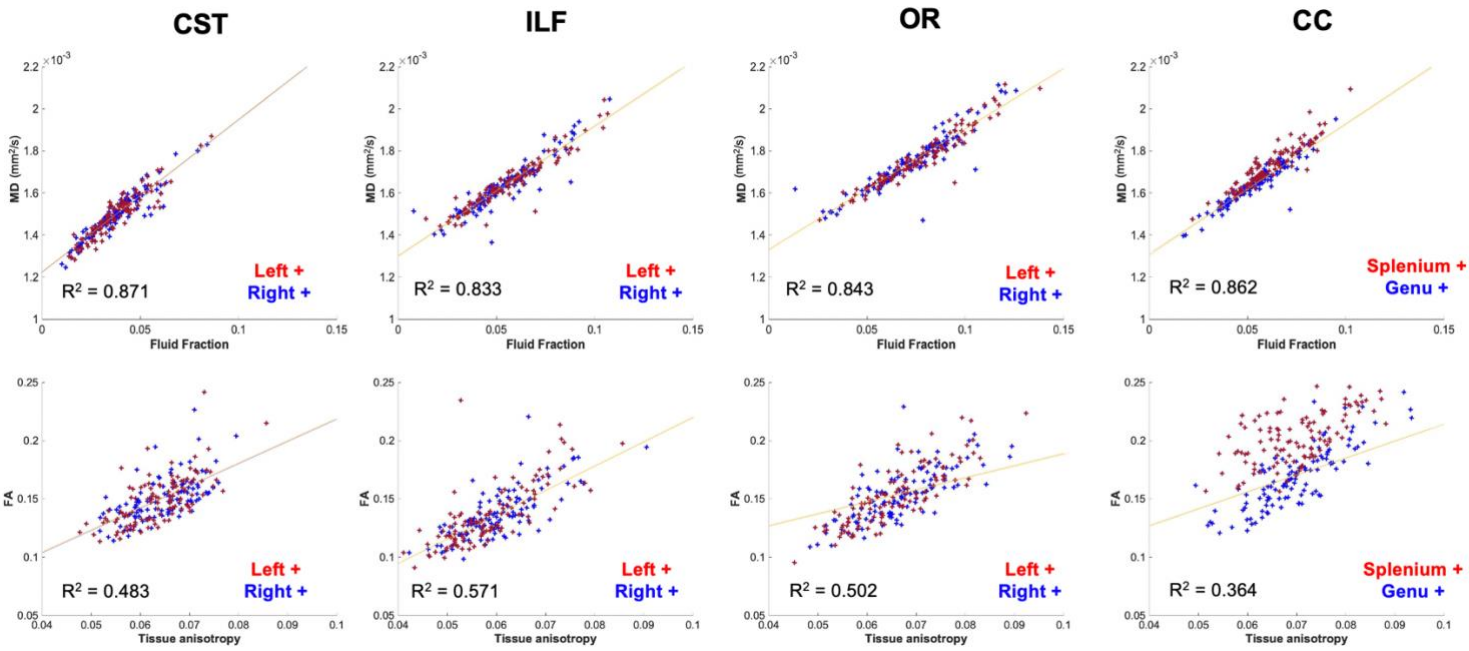

Figure 4. Top row: partial correlations between tract-average MD and volume fraction of the fluid component (significant relationship for all partial correlations, $p < 0.01$). Bottom row: Mean FA value of the tract plotted against the square root of the power in the l=2 band of the tissue component (tissue anisotropy) values in voxels traversed by each tract (significant relationship for all partial correlations, $p < 0.05$).